Check for updates

Construction of stable core–shell imprinted Ag-(poly-*o*-phenylenediamine)/CoFe$_2$O$_4$ photocatalyst endowed with the specific recognition capability for selective photodegradation of ciprofloxacin†

Ziyang Lu,[ab] Zehui Yu,[a] Jinbo Dong,[c] Minshan Song,[d] Yang Liu,[e] Xinlin Liu,[f] Di Fan,[c] Zhongfei Ma,[a] Yongsheng Yan [ID] *[b] and Pengwei Huo*[b]

A stable core–shell imprinted Ag-(poly-*o*-phenylenediamine)/CoFe$_2$O$_4$ (imprinted Ag-POPD/CoFe$_2$O$_4$) was synthesized *via* the surface imprinting technique. Ag-POPD was introduced into an imprinted layer, which significantly enhanced the photocatalytic activity. Meanwhile, due to the existence of imprinted cavities in the imprinted layer, the imprinted Ag-POPD/CoFe$_2$O$_4$ exhibited the superior specific recognition capability for selective photodegradation of ciprofloxacin (CIP). This work puts forward a novel design idea for synthesizing imprinted photocatalysts.

Introduction

In recent years, the development of industrialization has also been accompanied by increasingly serious environmental problems, especially water pollution.[1–5] Currently, due to the large usage of ciprofloxacin (CIP, one of the most common antibiotics), the harm caused by CIP residues to the ecological environment and human health is causing widespread concern.[6–9] Therefore, finding a simple, quick and effective method to remove CIP residues from the water environment is of great importance.[10–13] In this context, photocatalysis, as a green technology which uses light energy and degrades pollutants to non-toxic harmless substances, has aroused great interest among many researchers.[14–18]

Recently, TiO$_2$, CdS, ZnO and other materials have been extensively studied and widely used as photocatalysts.[19–23] They each have their respective advantages; however, their common shortcomings are also evident, such as poor selectivity, namely,

these common photocatalysts cannot selectively remove specific pollutants in the presence of other pollutants.[24–27] This inherent defect greatly limits their functional application. In order to overcome the above defect, the surface imprinting technique is widely used to improve the selectivity. Surface imprinting is an effective approach for synthesizing materials with the specific recognition capability towards the target molecule.[28–34]

Nevertheless, when these common photocatalysts are coated with an imprinted layer, although the selectivity will increase, the photocatalytic activity will greatly decrease due to the coating of the imprinted layer. Therefore, to improve selectivity without reducing photocatalytic activity is a major challenge. Based on the above considerations, we have found that poly-*o*-phenylenediamine (POPD, a typical conductive polymer)[35–37] can not only be used in the same way as the functional monomer for synthesizing the imprinted layer, but also possesses good photocatalytic activity. More importantly, the introduction of POPD into the imprinted layer can effectively avoid the decrease of photocatalytic activity resulting from the coating of an imprinted layer on common photocatalysts. Moreover, in order to further enhance the photocatalytic activity, silver (Ag)[38–42] can be loaded onto the POPD, in order to aid the transfer of photo-generated electrons from POPD. In brief, the introduction of Ag-POPD into the imprinted layer not only improves the selectivity, but also improves the photocatalytic activity.

On the other hand, the poor recycling capacity of the above imprinted material severely restricts its development and application.[43–45] CoFe$_2$O$_4$, as a widely used magnetic material, can be easily collected using a magnet without additional centrifugation or filtration and maintains a very good

[a]School of the Environment and Safety Engineering, Jiangsu University, Jiangsu, Zhenjiang 212013, PR China

[b]School of Chemistry & Chemical Engineering, Jiangsu University, Jiangsu, Zhenjiang 212013, PR China. E-mail: luziyang126@126.com; huopw@mail.ujs.edu.cn

[c]Zhenjiang Water Corporation, Jiangsu, Zhenjiang 212003, PR China

[d]School of Mathematics and Physics, Jiangsu University of Science and Technology, Jiangsu, Zhenjiang 212003, PR China

[e]Key Laboratory of Functional Materials Physics and Chemistry of the Ministry of Education, Jilin Normal University, Jilin, Changchun 130103, PR China

[f]School of Energy and Power Engineering, Jiangsu University, Jiangsu, Zhenjiang 212013, PR China

† Electronic supplementary information (ESI) available. See DOI: 10.1039/c7ra09835a

recyclability.[46–51] $CoFe_2O_4$ can be used not only as a carrier to improve the specific surface area of composite materials, but also can reduce the costs to improve the economic viability of composite materials.

Therefore, in this work, a stable core–shell imprinted Ag-(poly-o-phenylenediamine)/$CoFe_2O_4$ photocatalyst (imprinted Ag-POPD/$CoFe_2O_4$) was synthesized, based on $CoFe_2O_4$ as the carrier, via the surface imprinting technique. A series of characterizations were performed and influential factors were investigated to confirm the composition, structure, morphology and performance. The material properties in terms of adsorption, photocatalysis, selectivity, mechanism and reproducibility were also experimentally investigated.

Experimental section

Materials

Ferric chloride hydrate ($FeCl_3 \cdot 6H_2O$, A.R.), cobalt chloride hexahydrate ($CoCl_2 \cdot 6H_2O$, A.R.), ammonium acetate (A.R.), o-phenylenediamine (OPD, A.R.), trimethylpropane trimethacrylate (TRIM, A.R.) tert-butyl alcohol (t-BuOH, A.R.), triethanolamine (TEOA, A.R.) and benzoquinone (BQ, A.R.) were supplied by Aladdin Chemistry Co., Ltd. 2,2′-Azobis(2,4-dimethylvaleronitrile) (97%) was supplied by J&K Scientific Ltd. Ciprofloxacin (CIP, 99%) and tetracycline (TC, 99%) were purchased from National Institutes for Food and Drug Control. Trichloromethane (A.R.), sodium borohydride ($NaBH_4$, A.R.), ethylene glycol (A.R.), ammonium persulfate (A.R.), methanol (A.R.), anhydrous ethanol (A.R.), silver nitrate ($AgNO_3$, A.R.) and dimethyl sulfoxide (DMSO, A.R.) were all purchased from Sinopharm Chemical Reagent Co., Ltd. Nitrogen (N_2) was supplied by INHONG GAS. Deionized water was used throughout this work.

Synthesis

Synthesis of $CoFe_2O_4$. $CoFe_2O_4$ was synthesized as follows: 4 mmol of $FeCl_3 \cdot 6H_2O$ and 2 mmol of $CoCl_2 \cdot 6H_2O$ were dissolved in 70 mL of ethylene glycol. After a clear solution was formed, 30 mL of ammonium acetate was added into the above mixed solution with mechanical agitation for 30 min at 30 °C. Afterwards, the mixed solution was transferred into a Teflon-lined stainless steel autoclave and sealed to heat at 210 °C. After reacting for 48 h, the autoclave was cooled to room temperature. Subsequently, the solid product was washed with deionized water and anhydrous ethanol several times. Finally, after drying under vacuum at 50 °C, $CoFe_2O_4$ was obtained.

Synthesis of Ag-POPD. Briefly, 0.02 mol of OPD was dissolved in 30 mL of trichloromethane, which was marked as Sol. A. Meanwhile, 0.01 mol of ammonium persulfate was dissolved in 30 mL of deionized water. Then, the ammonium persulfate solution was slowly added into Sol. A. After the mixed solution was left to stand for 24 h, the product was washed with methanol and anhydrous ethanol several times. Finally, after drying under vacuum at 50 °C, poly-o-phenylenediamine (POPD) was obtained. In the following step, Ag-POPD was synthesized as follows: 1.45 g of POPD was added into 320 mL of 0.025 mol L^{-1}

$AgNO_3$ solution with mechanical agitation for 60 min at 30 °C. Afterwards, 380 mL of 0.025 mol L^{-1} $NaBH_4$ solution was added into the above mixed solution drop by drop. After reacting for 90 min under mechanical agitation, the product was washed with deionized water several times and then dried under vacuum at 50 °C. In consequence, Ag-POPD was obtained.

Synthesis of imprinted Ag-POPD/$CoFe_2O_4$. Imprinted Ag-POPD/$CoFe_2O_4$ was synthesized via the surface imprinting technique, by the following specific process: 0.5 g of $CoFe_2O_4$ and a certain amount of Ag-POPD were added into 50 mL of DMSO. After reacting for 60 min under magnetic stirring at 30 °C, 0.05 g of ciprofloxacin (CIP) was added into this solution, and the reaction was continued for another 60 min under magnetic stirring at 30 °C. Subsequently, 0.5 mL of TRIM and 0.005 g of 2,2′-azobis(2,4-dimethylvaleronitrile) were both added into the above mixed solution. Then, the polymerization reaction was carried out in a microwave synthesizer (XH-300UL, Beijing XiangHu Science and Technology Development Co., Ltd) at 600 W and 40 °C under a N_2 atmosphere. After reacting for a period of time, the product was washed with deionized water and anhydrous ethanol several times. Afterwards, the molecular template (CIP) was removed by adding 200 mL deionized water into the above solution under simulated sunlight irradiation (250 W xenon lamp) for 3 h with magnetic agitation at 30 °C under an air atmosphere. Finally, the solid product was washed with deionized water and anhydrous ethanol several times. After drying under vacuum at 50 °C, imprinted Ag-POPD/$CoFe_2O_4$ was obtained. The general scheme of the synthesis approach is shown in Scheme 1.

Synthesis of non-imprinted Ag-POPD/$CoFe_2O_4$. The synthesis process of non-imprinted Ag-POPD/$CoFe_2O_4$ was consistent with that of imprinted Ag-POPD/$CoFe_2O_4$, but without the addition and removal process of CIP.

Characterization

Fourier-transformed infrared (FT-IR) spectra of the samples were recorded on a Nicolet Nexus 470 FT-IR (Thermo Nicolet Co., USA) with 2.0 cm^{-1} resolution in the range 400–4000 cm^{-1}, using KBr pellets. X-ray photoelectron spectroscopy (XPS) was measured with a PHI5300 spectrometer using an Al Kα (12.5 kV) X-ray source. XRD patterns were obtained with a D8 ADVANCE X-ray diffractometer (Bruker AXS Co., Germany). The morphology was observed by a JEM-2010 transmission electron microscope (TEM, Japan) and a JSM-7001F scanning electron microscope (SEM, Japan) equipped with energy dispersive spectroscopy analysis (EDS). UV-vis diffuse reflectance spectra (UV-vis DRS) were obtained for the dry-pressed disk samples using a 2450 spectrometer (Shimadzu Co., Japan) equipped with the integrated sphere accessory for diffuse reflectance spectra, using $BaSO_4$ as the reflectance sample. The specific surface area, pore volume and average pore diameter of the samples were measured by using a NOVA 4000e high speed automated surface area and pore size analyzer (Quantachrome Co., USA). Magnetic measurement was carried out using a vibrating sample magnetometer (VSM) (7300, Lakeshore) under a magnetic field up to 10 kOe. The photoluminescence (PL)
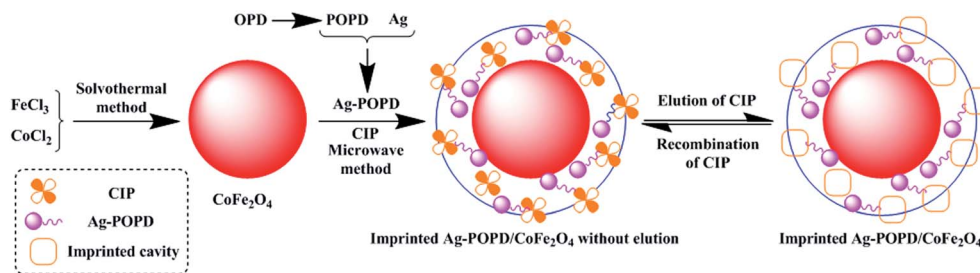
Scheme 1 General scheme of the synthesis approach.

spectra of different samples were investigated by utilizing a fluorescence spectrophotometer (Cary Eclipse Spectrophotometer, VARIAN, USA) equipped with a xenon lamp as the excitation source at room temperature with an excitation wavelength of 253 nm.

Experiments of adsorption, photocatalysis, selectivity, mechanism and reproducibility

The adsorption experiment was carried out with magnetic stirring (600 rpm) at 25 °C in the dark. Briefly, 0.1 g of sample was added into 100 mL of 10 mg L^{-1} CIP solution. Subsequently, the sample analysis was carried out at intervals of 10 min. After 60 min in the dark, the solid sample was isolated using a magnet, and the concentration was measured with a UV-vis spectrophotometer 2450 (Shimadzu Co., Japan). The adsorption capacity (Q) was calculated by using the formula:

$$Q = \frac{(C_0 - C) \times V}{m} \quad (1)$$

where C_0 was the initial concentration of CIP, C was the concentration of CIP after adsorption, V was the volume of the CIP solution, and m was the mass of the sample.

The photocatalytic experiment was carried out at 25 °C with magnetic stirring (600 rpm) under an air atmosphere (the aeration rate was 2 mL min^{-1}) and simulated sunlight irradiation provided by a 250 W xenon lamp (the illuminance reached 1.8×10^5 lux). Briefly, 0.1 g of sample was added into 100 mL of 10 mg L^{-1} CIP solution. After reaching the desired adsorption time in the dark, the initial concentration was determined. Subsequently, the sample analysis was carried out at intervals of 15 min. After exposure to simulated sunlight irradiation for 60 min, the concentration was measured with the UV-vis spectrophotometer 2450. The photodegradation degree was calculated by using the formula:

$$\text{Photodegradation degree} = 1 - \frac{C}{C_0} \times 100\% \quad (2)$$

where C_0 was the initial concentration of CIP after adsorption and C was the concentration of CIP after photodegradation reaction.

The selectivity experiment was carried out in accordance with the photocatalytic experiment, but during the reaction process, 0.1 g of sample was added into 100 mL of 20 mg L^{-1} tetracycline (TC) solution, and the concentration was likewise measured with the UV-vis spectrophotometer 2450. The selectivity coefficient ($k_{\text{selectivity}}$) was calculated by using the following formulas:

For the imprinted sample:

$$k_{\text{imprinted}} = \frac{\text{photodegradation degree (CIP)}}{\text{photodegradation degree (TC)}} \quad (3)$$

For other samples:

$$k_{\text{others}} = \frac{\text{photodegradation degree (CIP)}}{\text{photodegradation degree (TC)}} \quad (4)$$

For the selectivity coefficient:

$$k_{\text{selectivity}} = \frac{k_{\text{imprinted}}}{k_{\text{others}}} \quad (5)$$

In order to investigate the dominant reactive oxygen species and mechanism of degradation of CIP with the imprinted Ag-POPD/CoFe$_2$O$_4$, the corresponding experiments were also carried out in accordance with the above photocatalytic experiment, but with the following difference: at the beginning of the photocatalytic reaction, various quenchers (1 mmol) were added into the CIP solution, including *tert*-butyl alcohol (t-BuOH), triethanolamine (TEOA) and benzoquinone (BQ).

The reproducibility of the imprinted Ag-POPD/CoFe$_2$O$_4$ was investigated as follows: after the first photocatalytic reaction, the sample was isolated by a magnet and sonicated with anhydrous ethanol for 1 h to remove the residual CIP and by-products. After the product was washed with deionized water and dried, it was used to perform another photocatalytic reaction. The above procedure was repeated five times to confirm the reproducibility of the imprinted Ag-POPD/CoFe$_2$O$_4$.

Results and discussion

Characterization

The first task was to record the XRD patterns of different samples, which are shown in Fig. S2.† As can be clearly seen in Fig. S2a,† the XRD pattern matched the face-centered cubic structure of Ag (JCPDS standard card 65-2871): the diffraction peaks observed at $2\theta = 38.1°$, 44.3°, 64.4° and 77.4° corresponded to the indexes (111), (200), (220) and (311) for Ag,[52,53] which indicated that Ag had been successfully loaded on POPD.

Meanwhile, in Fig. S2b,† the diffraction peaks appearing at 2θ values of 30.1°, 35.4°, 37.1°, 43.1°, 53.4°, 56.9°, 62.5°, 70.9°, 73.9° and 74.9° correspond to the indexes (220), (311), (222), (400), (422), (511), (440), (620), (533) and (622) of the cubic $CoFe_2O_4$ with a spinel structure, and closely match the JCPDS standard card 22-1086 data file.[46,48,54] In addition, the XRD patterns of imprinted Ag-POPD/$CoFe_2O_4$ and non-imprinted Ag-POPD/$CoFe_2O_4$ not only possessed all the characteristic diffraction peaks of $CoFe_2O_4$, but also a strong and unambiguous diffraction peak of Ag, while no other diffraction peaks were observed in these two patterns. The results indicated that the crystalline structures of $CoFe_2O_4$ and Ag were not changed during coating of the outer layer.

In order to further confirm the elemental composition of imprinted Ag-POPD/$CoFe_2O_4$, XPS spectra were recorded, as shown in Fig. 1. It could be clearly seen that the C 1s pattern showed a dominant peak at 283.75 eV, accompanied by two minor peaks at 285.31 eV and 286.53 eV, which were assigned to C=C, C–O and –COO groups, respectively.[36] The four component peaks of N 1s were attributed to pyridinic N (398.71 eV), nitrile N or imine N (399.41 eV), pyrrolic N (400.41 eV) and graphitic N (401.31 eV).[35,36] The peaks at 530.2 eV, 531.2 eV, 532.2 eV and 534.2 eV were assigned to adsorbed oxygen, =C=O/–C–O–C–, –O–C=O and –N–O–, respectively.[35,36] All the above peaks confirmed that POPD was successfully synthesized. Furthermore, Ag $3d_{5/2}$ (368.69 eV) and Ag $3d_{3/2}$ (374.79 eV) were observed in the sample, indicating that the as-prepared sample possessed Ag.[54] Moreover, the peaks at 779.64 eV (with a satellite peak at 784.83 eV) and at 798.61 eV (with a satellite peak at 804.23 eV) correspond to Co $2p_{3/2}$ and Co $2p_{1/2}$, respectively, and are the characteristic peaks of Co^{2+}.[54] At the same time, Fe $2p_{3/2}$ (711.29 eV) and Fe $2p_{1/2}$ (723.49 eV) were observed in the sample.[54] The presence of Co $2p_{3/2}$, Co $2p_{1/2}$, Fe $2p_{3/2}$ and Fe $2p_{1/2}$ indicated that $CoFe_2O_4$ was present in the as-prepared sample. Therefore, all the above results confirmed that the imprinted Ag-POPD/$CoFe_2O_4$ was successfully synthesized.

Fig. 2 presents the FT-IR spectra of $CoFe_2O_4$ and imprinted Ag-POPD/$CoFe_2O_4$, which were recorded to further verify the formation of imprinted Ag-POPD/$CoFe_2O_4$. Compared with $CoFe_2O_4$, due to the formation of the imprinted layer and the introduction of POPD, some additional absorption peaks (1668 cm^{-1}, 1523 cm^{-1}, 1481 cm^{-1}, 1384 cm^{-1}, 1295 cm^{-1}, 1189 cm^{-1}, 949 cm^{-1} and 893 cm^{-1}) were observed in imprinted Ag-POPD/$CoFe_2O_4$. The absorption peak at 1668 cm^{-1} was attributed to the stretching vibration of C=O,[16] the absorption peak of C=C was observed at 1523 cm^{-1},[55] the absorption peak at 1481 cm^{-1} was assigned to the skeleton vibration peaks of the benzene ring,[16] the absorption peaks of C–N–C were observed at 1384 cm^{-1} and 1295 cm^{-1},[55] the absorption peak of C–C was observed at 1189 cm^{-1},[55] and the absorption peaks of C–H were observed at 949 cm^{-1} and 893 cm^{-1}. All the above absorption peaks indicated that POPD and the imprinted layer were successfully formed in imprinted Ag-POPD/$CoFe_2O_4$, and the imprinted Ag-POPD/$CoFe_2O_4$ had been successfully synthesized.

TEM images, SEM images and EDS spectra of $CoFe_2O_4$ and imprinted Ag-POPD/$CoFe_2O_4$ are shown in Fig. 3 and S3.† Fig. 3a and c display that $CoFe_2O_4$ possessed a good spherical structure with an average diameter of approximately 500 nm. The presence of the elements O, Fe and Co, as indicated in Fig. S3a,† confirmed again that $CoFe_2O_4$ had been successfully synthesized. Compared with Fig. 3a, a surface coating layer can be clearly observed in Fig. 3b, which indicates that the surface imprinted layer had been successfully coated on the surface of $CoFe_2O_4$. It can be clearly seen from Fig. 3b and d that after coating the surface imprinted layer, the imprinted Ag-POPD/$CoFe_2O_4$ still possessed good spherical and core–shell structure,
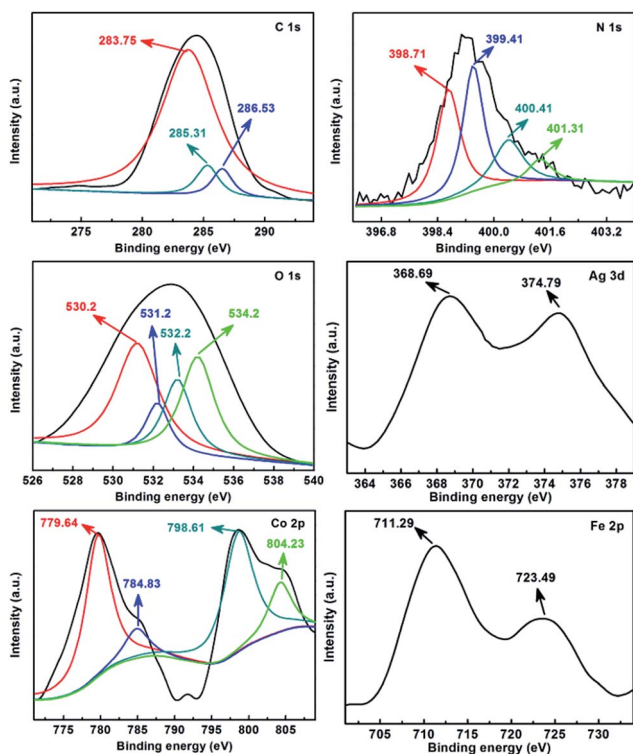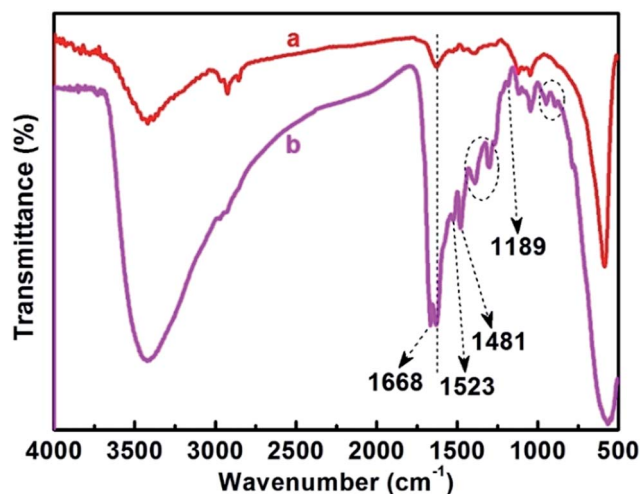

Fig. 1 XPS spectra of imprinted Ag-POPD/$CoFe_2O_4$.

Fig. 2 FT-IR spectra of different samples ((a) $CoFe_2O_4$ and (b) imprinted Ag-POPD/$CoFe_2O_4$).
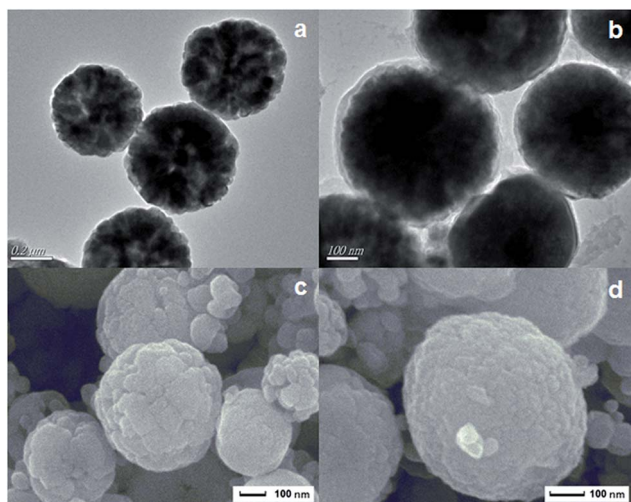
Fig. 3 TEM images and SEM images of $CoFe_2O_4$ (a and c) and imprinted Ag-POPD/$CoFe_2O_4$ (b and d).

and the average diameter was approximately 530 nm. Furthermore, compared with Fig. S3a,† the additional elements C and Ag are observed in Fig. S3b,† which verifies again that Ag-POPD and the imprinted layer were both present in the imprinted Ag-POPD/$CoFe_2O_4$.

In order to further confirm that the imprinted cavities were indeed present in the imprinted layer, N_2 adsorption–desorption experiments were carried out. As shown in Fig. 4, it could be clearly seen that the N_2 adsorption–desorption isotherm of imprinted Ag-POPD/$CoFe_2O_4$ displayed the type IV behavior with distinct hysteresis loops consistent with the H1 type, demonstrating that the imprinted Ag-POPD/$CoFe_2O_4$ possessed a mesoporous structure.[56,57] The BET specific surface area reached 199.09 m^2 g^{-1} and the average pore diameter obtained from the Barrett–Joyner–Halenda (BJH) method was 2.61 nm. Furthermore, as shown in Fig. S4,† compared with imprinted Ag-POPD/$CoFe_2O_4$, the non-imprinted Ag-POPD/$CoFe_2O_4$
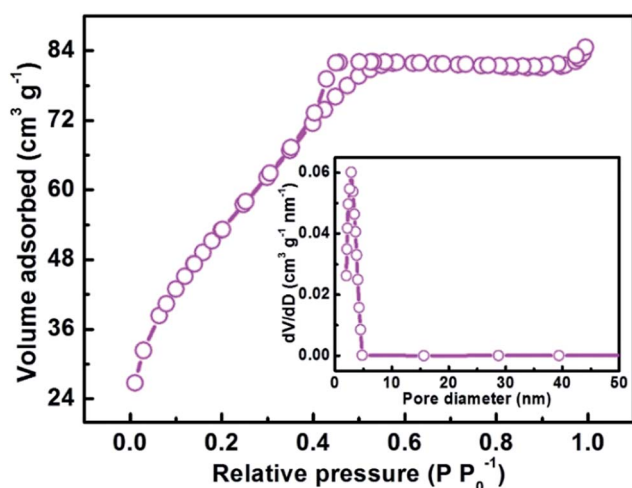
possessed a very small BET specific surface area (9.47 m^2 g^{-1}) and a large average pore diameter (28.93 nm), due to the fact that no imprinted cavities were present in the non-imprinted Ag-POPD/$CoFe_2O_4$. Therefore, the N_2 adsorption–desorption experiments conclusively proved that imprinted cavities were formed in the imprinted layer of imprinted Ag-POPD/$CoFe_2O_4$.

Fig. 5 and S5† show the UV-vis DRS spectra and the magnetization patterns at room temperature of $CoFe_2O_4$ and imprinted Ag-POPD/$CoFe_2O_4$. As shown in Fig. 5, after coating the imprinted layer and introducing Ag-POPD, imprinted Ag-POPD/$CoFe_2O_4$ exhibited good absorption across a wide range of light wavelengths, which indicated that the imprinted Ag-POPD/$CoFe_2O_4$ had a favorable response to light. Moreover, Fig. S5† shows that the magnetic saturation (M_s) value of $CoFe_2O_4$ was 69.08 emu g^{-1}, which represents distinct magnetism. Moreover, even after coating the imprinted layer, the magnetic saturation (M_s) value of imprinted Ag-POPD/$CoFe_2O_4$ was 65.82 emu g^{-1}, which showed that the distinct magnetism was not significantly reduced. From the photograph (inset in Fig. 5), it could be clearly observed that the imprinted Ag-POPD/$CoFe_2O_4$ could be easily separated by a magnet, indicating that the imprinted Ag-POPD/$CoFe_2O_4$ indeed possessed good magnetic separation performance.

Adsorption, photocatalytic activity, selectivity and reproducibility

As shown in Fig. 6, the adsorption performance of different samples was investigated. For the first 30 min of adsorption, the adsorption capacity of $CoFe_2O_4$, Ag-POPD, imprinted Ag-POPD/$CoFe_2O_4$ and non-imprinted Ag-POPD/$CoFe_2O_4$ increased significantly. After 30 min of adsorption, the reaction process, which followed the order of adsorption–desorption–adsorption, reached the equilibrium adsorption state for photocatalysis. At this time, the value of the adsorption capacity of $CoFe_2O_4$, Ag-POPD, imprinted Ag-POPD/$CoFe_2O_4$ and non-imprinted Ag-
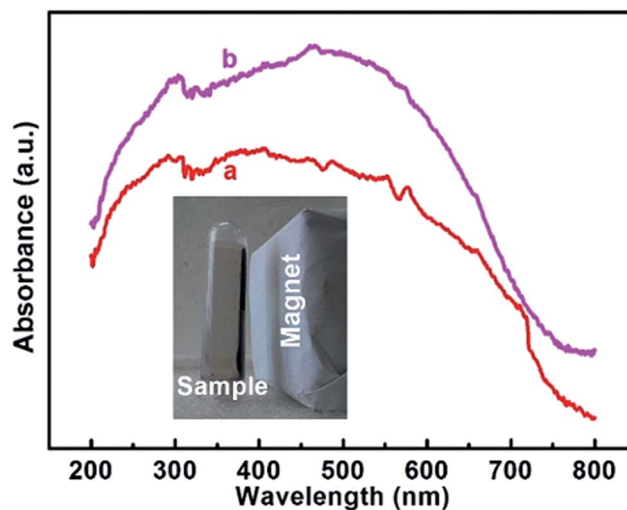

Fig. 4 N_2 adsorption–desorption isotherm and corresponding pore size distribution curve (inset) of the imprinted Ag-POPD/$CoFe_2O_4$.

Fig. 5 UV-vis DRS spectra of $CoFe_2O_4$ (a) and imprinted Ag-POPD/$CoFe_2O_4$ (b) (inset is the photograph of the imprinted Ag-POPD/$CoFe_2O_4$ separated from solution under a magnet).
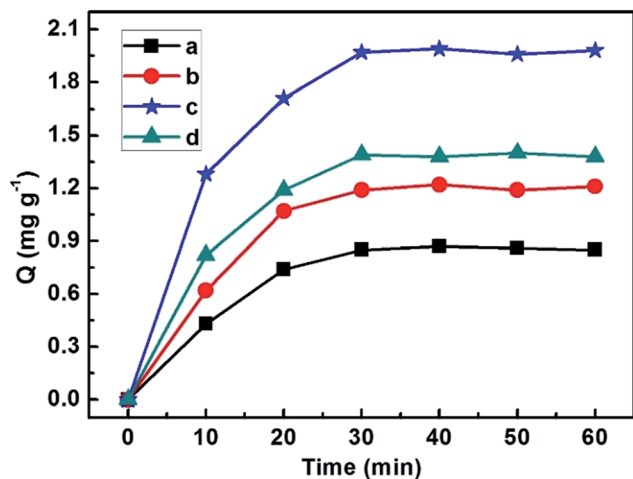
Fig. 6 Adsorption capacities of different samples ((a) $CoFe_2O_4$, (b) Ag-POPD, (c) imprinted Ag-POPD/$CoFe_2O_4$ and (d) non-imprinted Ag-POPD/$CoFe_2O_4$).

POPD/$CoFe_2O_4$ fluctuated around 0.85 mg g^{-1}, 1.21 mg g^{-1}, 1.98 mg g^{-1} and 1.38 mg g^{-1}, respectively. The above results indicated that compared with $CoFe_2O_4$, Ag-POPD and non-imprinted Ag-POPD/$CoFe_2O_4$, imprinted Ag-POPD/$CoFe_2O_4$ exhibited the highest adsorption performance, because of the existence of a large number of imprinted cavities in the imprinted layer of imprinted Ag-POPD/$CoFe_2O_4$, which had a strong specific recognition capability for selective adsorption of CIP. Therefore, in the following experiments, 30 min was chosen as the desired adsorption time.

In order to achieve a better photocatalytic activity, the influences of different additive doses of Ag-POPD and different microwave polymerization times on the photocatalytic activity of the imprinted Ag-POPD/$CoFe_2O_4$ were investigated, as shown in Fig. 7. In Fig. 7A, when the additive dose of Ag-POPD was 0.1 g, the imprinted Ag-POPD/$CoFe_2O_4$ possessed the highest photocatalytic activity (94.38%). When the additive dose of Ag-POPD was lower than 0.1 g, the content of Ag-POPD was below the optimum value, resulting in lower photocatalytic activity. Meanwhile, when the additive dose of Ag-POPD was

higher than 0.1 g, the excessive Ag-POPD led to a lower density of imprinted cavities in the imprinted layer. Thus, the distribution of imprinted cavities on the surface became less dense, which in turn led to a decrease in photocatalytic activity. Hence 0.1 g was the optimum additive dose of Ag-POPD. Furthermore, as shown in Fig. 7B, the optimum microwave polymerization time was 60 min: under these conditions, the photodegradation degree reached 94.38%. When the microwave polymerization time was lower than 60 min, the polymerization was not complete, namely, the imprinted layer had not been fully formed, resulting in low photocatalytic activity. Meanwhile, when the microwave polymerization time was higher than 60 min, the degree of microwave polymerization was too high: on one hand, the imprinted layer became thicker, and the distribution of imprinted cavities on the surface became less dense, while on the other hand, the bonding became more stable, which was detrimental to the removal and re-binding of CIP. The above two factors both led to low photocatalytic activity. Therefore, in the following experiments, 0.1 g was chosen as the additive dose of Ag-POPD, and 60 min was chosen as the microwave polymerization time.

The selectivity of different samples was investigated by comparing the photodegradation degree for degradation of CIP and TC, as displayed in Fig. 8. It could be clearly seen that the photocatalytic activity of $CoFe_2O_4$ was very low, possibly implying that degradation mainly relied on the adsorption and self-degradation of CIP and TC. Furthermore, for photodegradation of CIP, imprinted Ag-POPD/$CoFe_2O_4$ possessed a large number of imprinted cavities in the imprinted layer and these imprinted cavities had strong affinity to CIP, enabling them to specifically recognize and selectively photodegrade CIP. Hence, imprinted Ag-POPD/$CoFe_2O_4$ achieved the highest photodegradation degree (94.38%) in 90 min under simulated sunlight irradiation, which was approximately 5.47 times that of $CoFe_2O_4$, 1.34 times that of Ag-POPD and 1.29 times that of non-imprinted Ag-POPD/$CoFe_2O_4$. On the other hand, because of the relatively large structural difference between CIP and TC, the imprinted cavities could not efficiently specifically recognize TC. Therefore, for photodegradation of TC, compared with Ag-POPD and non-imprinted Ag-POPD/$CoFe_2O_4$, imprinted Ag-
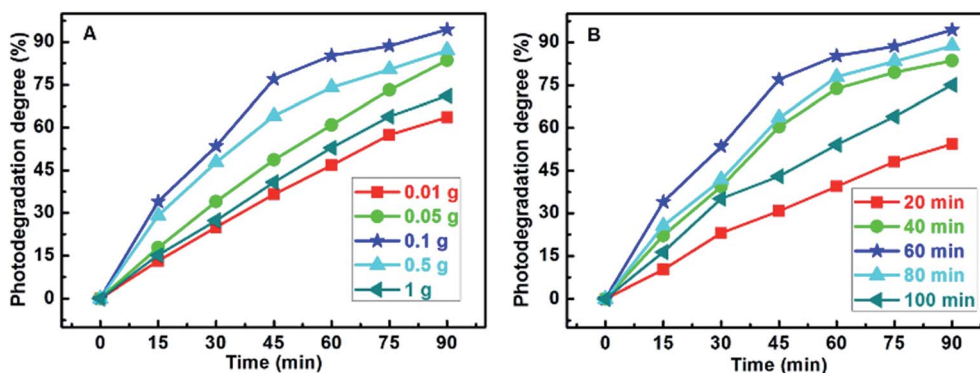

Fig. 7 Influence of different additive doses of Ag-POPD (A) and influence of different microwave polymerization times (B) on photocatalytic activity of the imprinted Ag-POPD/$CoFe_2O_4$.
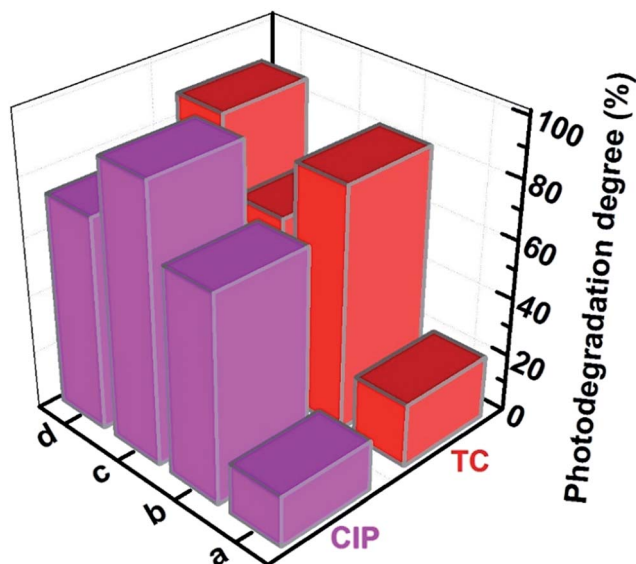
Fig. 8 Selectivity for degradation of different pollutants with different samples under simulated sunlight irradiation for 90 min ((a) $CoFe_2O_4$, (b) Ag-POPD, (c) imprinted Ag-POPD/$CoFe_2O_4$ and (d) non-imprinted Ag-POPD/$CoFe_2O_4$).

POPD/$CoFe_2O_4$ achieved a relatively poor photodegradation degree (62.75%) in 90 min under simulated sunlight irradiation.

In addition, Table 1 presents the detailed photodegradation degrees and coefficients of selectivity of the different photocatalysts. The coefficient of selectivity ($k_{selectivity}$) of imprinted Ag-POPD/$CoFe_2O_4$ relative to $CoFe_2O_4$, Ag-POPD and non-imprinted Ag-POPD/$CoFe_2O_4$ was 1.88, 1.79 and 1.83, respectively. These values of $k_{selectivity}$ indicated that imprinted Ag-POPD/$CoFe_2O_4$ was highly selective for the structure of CIP as a result of the imprinted cavities, which could selectively photodegrade CIP in the presence of TC. Therefore, all the above results demonstrated that imprinted Ag-POPD/$CoFe_2O_4$ not only had high photocatalytic efficiency, but also possessed the specific recognition capability for selective photodegradation of CIP.

The reproducibility of imprinted Ag-POPD/$CoFe_2O_4$ was investigated by performing 5 cycles of use, as shown in Fig. S6.† It could be clearly seen that the imprinted Ag-POPD/$CoFe_2O_4$ could be used for at least 5 cycles with little loss of

photocatalytic activity, demonstrating that the imprinted Ag-POPD/$CoFe_2O_4$ had good photocatalytic stability and reproducibility. Furthermore, Fig. S6B† shows that the XRD pattern of the sample after 5 cycles was nearly the same as that of the initial sample, demonstrating that the crystalline structure of imprinted Ag-POPD/$CoFe_2O_4$ was not changed during the photocatalytic reaction. In addition, the photoluminescence (PL) spectra[58,59] were further investigated to confirm the reproducibility, as shown in Fig. S7.† It could be easily observed that the spectrum of imprinted Ag-POPD/$CoFe_2O_4$ was almost unchanged after 5 cycles, demonstrating that the as-prepared imprinted Ag-POPD/$CoFe_2O_4$ had good photocatalytic stability and reproducibility.

Dominant reactive oxygen species and mechanism

In order to investigate the photocatalytic mechanism of degradation of CIP with the imprinted Ag-POPD/$CoFe_2O_4$, photocatalytic experiments were performed in which TEOA, t-BuOH or BQ were used as quenchers for h^+, $\cdot OH$, and $\cdot O_2^-$, respectively. The results are shown in Fig. 9. When t-BuOH and BQ were added into the CIP solution, the photodegradation degree was reduced to 79.29% and 64.88%, respectively, compared with that without quencher (94.38%), which indicated that t-BuOH and BQ had little effect on the photocatalytic activity of
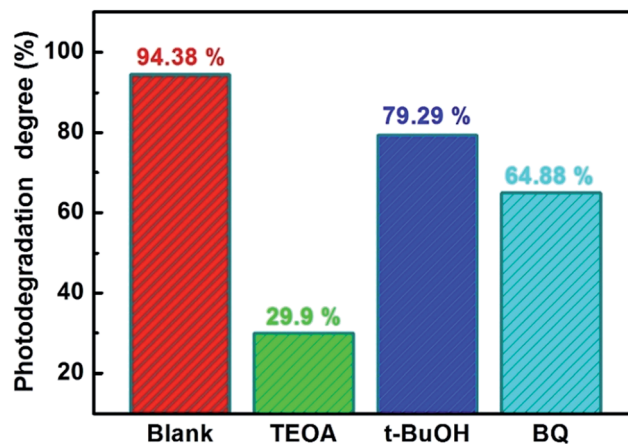

Fig. 9 Photodegradation degrees for degradation of CIP with the imprinted Ag-POPD/$CoFe_2O_4$ in the presence of different quenchers under simulated sunlight irradiation for 90 min.

Table 1 Photodegradation degrees and coefficients of selectivity with different photocatalysts under simulated sunlight irradiation for 90 min

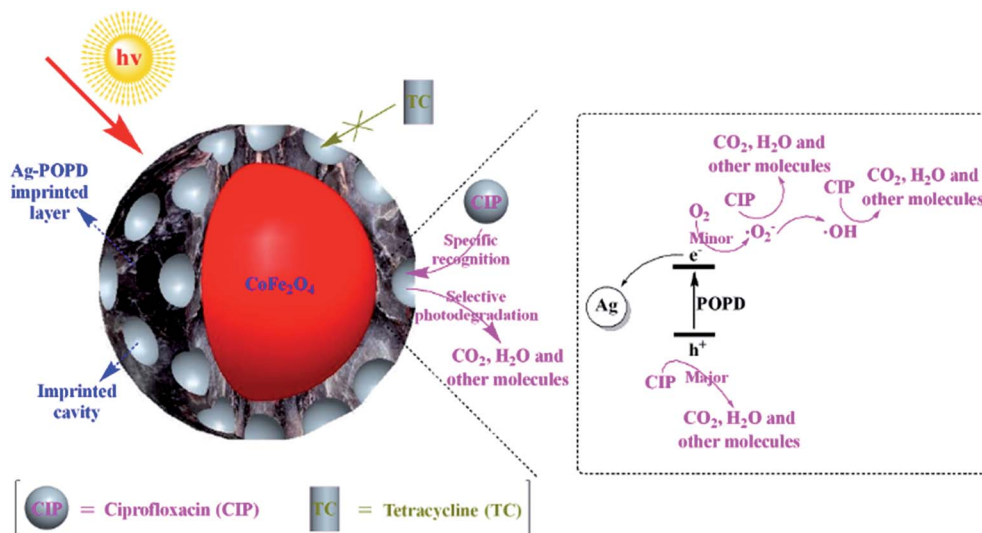| Photocatalysts	Antibiotic solution	Photodegradation degrees (%)	$k_{imprinted}$	k_{others}	$k_{selectivity}$
$CoFe_2O_4$	CIP	17.25	—	0.8	1.88
	TC	21.68			
Ag-POPD	CIP	70.41	—	0.84	1.79
	TC	83.61			
Imprinted Ag-POPD/$CoFe_2O_4$	CIP	94.38	1.5	—	—
	TC	62.75			
Non-imprinted Ag-POPD/$CoFe_2O_4$	CIP	73	—	0.82	1.83
	TC	88.61			

Fig. 10 Proposed selective photocatalytic mechanism of the imprinted Ag-POPD/CoFe$_2$O$_4$.

imprinted Ag-POPD/CoFe$_2$O$_4$. In contrast, when TEOA was added into the CIP solution, the photodegradation degree was heavily reduced to only 29.9%, indicating that TEOA exerted a significant effect on the photocatalytic activity of imprinted Ag-POPD/CoFe$_2$O$_4$. Therefore, in this photocatalytic reaction, h$^+$ was the main oxidative species, $^{\cdot}$O$_2^-$ was the secondary oxidative species, while $^{\cdot}$OH only played a small role. Based on the above results, we note that if h$^+$ had reacted with H$_2$O or OH$^-$ to form $^{\cdot}$OH in large amounts, $^{\cdot}$OH would have played a greater role. Hence, we draw the interesting conclusion that $^{\cdot}$OH was not formed in large amounts by the reaction of h$^+$ and H$_2$O/OH$^-$.

Combining all the above results, the selective photocatalytic mechanism of imprinted Ag-POPD/CoFe$_2$O$_4$ was proposed, as displayed in Fig. 10. Briefly, when imprinted Ag-POPD/CoFe$_2$O$_4$ was exposed to simulated sunlight, electrons (e$^-$) and holes (h$^+$) were generated in the LUMO energy level and the HOMO energy level of POPD. Afterwards, the majority of e$^-$ in the LUMO energy level of POPD transferred to Ag, while the remaining minority of e$^-$ in the LUMO energy level of POPD were captured by dissolved O$_2$ to generate superoxide radicals ($^{\cdot}$O$_2^-$), which further generated hydroxyl radicals ($^{\cdot}$OH). The $^{\cdot}$O$_2^-$ and $^{\cdot}$OH that originated from O$_2$ played only a minor role in the photocatalytic reaction. Meanwhile, the h$^+$ could directly oxidize CIP to generate CO$_2$, H$_2$O and other molecules. In addition, CIP could be specifically recognized by the imprinted cavities in the imprinted layer, but TC could not. Therefore, the specific recognition and selective photodegradation of CIP was realized through the imprinted cavities.

Conclusions

In brief, based on CoFe$_2$O$_4$ as the carrier, an imprinted Ag-POPD/CoFe$_2$O$_4$ was synthesized *via* the surface imprinting technique, and possessed a spherical core–shell structure, strong response to light, good magnetic separation performance and good reproducibility. Moreover, when the additive dose of Ag-POPD was 0.1 g and the microwave polymerization time was 60 min, the imprinted Ag-POPD/CoFe$_2$O$_4$ achieved the highest photodegradation degree (94.38%) for degradation of CIP in 90 min under simulated sunlight irradiation. Furthermore, Ag-POPD was introduced into the imprinted layer, which significantly enhanced the photocatalytic activity; meanwhile, due to the existence of imprinted cavities in the imprinted layer, the imprinted Ag-POPD/CoFe$_2$O$_4$ exhibited a superior specific recognition capability for selective photodegradation of CIP. In addition, in this photocatalytic reaction, h$^+$ was the main oxidative species, $^{\cdot}$O$_2^-$ was the secondary oxidative species, while $^{\cdot}$OH only played a small role.

Conflicts of interest

There are no conflicts to declare.

Acknowledgements

References

1 C. Santhosh, V. Velmurugan, G. Jacob, S. K. Jeong, A. N. Grace and A. Bhatnagar, *Chem. Eng. J.*, 2016, **306**, 1116–1137.

2 Z. Zhu, X. Tang, S. Kang, P. W. Huo, M. S. Song, W. D. Shi, Z. Y. Lu and Y. S. Yan, *J. Phys. Chem. C*, 2016, **120**, 27250–27258.

3 K. H. Chu, Y. A. J. Al-Hamadani, C. M. Park, G. Lee, M. Jang, A. Jang, N. Her, A. Son and Y. Yoon, *Chem. Eng. J.*, 2017, **327**, 629–647.

4 Z. Y. Lu, P. W. Huo, Y. Y. Luo, X. L. Liu, D. Wu, X. Gao, C. X. Li and Y. S. Yan, *J. Mol. Catal. A: Chem.*, 2013, **378**, 91–98.

5 G. G. Liu, K. Han, H. Q. Ye, C. Y. Zhu, Y. P. Gao, Y. Liu and Y. H. Zhou, *Chem. Eng. J.*, 2017, **320**, 74–80.

6 A. R. Silva, P. M. Martins, S. Teixeira, S. A. C. Carabineiro, K. Kuehn, G. Cuniberti, M. M. Alves, S. Lanceros-Mendez and L. Pereira, *RSC Adv.*, 2016, **6**, 95494–95503.

7 Z. Y. Lu, Z. Zhu, D. D. Wang, Z. F. Ma, W. D. Shi, Y. S. Yan, X. X. Zhao, H. J. Dong, L. Yang and Z. F. Hua, *Catal. Sci. Technol.*, 2016, **6**, 1367–1377.

8 B. X. Liu, Y. K. Huang, Q. Shen, X. Zhu, Y. Q. Hao, P. Qu and M. T. Xu, *RSC Adv.*, 2016, **6**, 100743–100747.

9 S. Martin, A. Shchukarev, K. Hanna and J. Boily, *Environ. Sci. Technol.*, 2015, **49**, 12197–12205.

10 Z. W. Zhao, J. H. Zhao and C. Yang, *Chem. Eng. J.*, 2017, **327**, 481–489.

11 Z. Y. Lu, X. X. Zhao, Z. Zhu, Y. S. Yan, W. D. Shi, H. J. Dong, Z. F. Ma, N. L. Gao, Y. S. Wang and H. Huang, *Chem.–Eur. J.*, 2015, **21**, 18528–18533.

12 M. F. Li, Y. G. Liu, S. B. Liu, D. Shu, G. M. Zeng, X. J. Hu, X. F. Tan, L. H. Jiang, Z. L. Yan and X. X. Cai, *Chem. Eng. J.*, 2017, **319**, 219–228.

13 A. Hassani, A. Khataee and S. Karaca, *J. Mol. Catal. A: Chem.*, 2015, **409**, 149–161.

14 C. Bojer, J. Schöbel, T. Martin, M. Ertl, H. Schmalz and J. Breu, *Appl. Catal., B*, 2017, **204**, 561–565.

15 X. B. Yang, J. Chen, H. X. Lai, J. P. Hu, M. Fang and X. T. Luo, *RSC Adv.*, 2017, **7**, 38519–38525.

16 Z. Y. Lu, Y. Y. Luo, M. He, P. W. Huo, T. T. Chen, W. D. Shi, Y. S. Yan, J. M. Pan, Z. F. Ma and S. Y. Yang, *RSC Adv.*, 2013, **3**, 18373–18382.

17 G. Z. Yuan, C. F. Hsia, Z. W. Lin, C. Chiang, Y. W. Chiang and M. H. Huang, *Chem.–Eur. J.*, 2016, **22**, 12548–12556.

18 Y. Y. Shao, W. D. Ye, C. Y. Sun, C. L. Liu and Q. Wang, *RSC Adv.*, 2017, **7**, 39089–39095.

19 Y. Xu, Z. C. Fu, S. Cao, Y. Chen and W. F. Fu, *Catal. Sci. Technol.*, 2017, **7**, 587–595.

20 Z. Y. Lu, W. C. Zhou, P. W. Huo, Y. Y. Luo, M. He, J. M. Pan, C. X. Li and Y. S. Yan, *Chem. Eng. J.*, 2013, **217**, 398–406.

21 S. N. Liu, M. Zheng, R. Chen and Z. S. Wang, *RSC Adv.*, 2017, **7**, 31230–31238.

22 Z. Zhu, X. Tang, C. C. Ma, M. S. Song, N. L. Gao, Y. S. Wang, P. W. Huo, Z. Y. Lu and Y. S. Yan, *Appl. Surf. Sci.*, 2016, **387**, 366–374.

23 H. W. Bai, Z. Y. Liu, L. Liu and D. D. Sun, *Chem.–Eur. J.*, 2013, **19**, 3061–3070.

24 Y. N. Zhang, W. G. Dai, Y. Z. Wen and G. H. Zhao, *Appl. Catal., B*, 2017, **212**, 185–192.

25 Z. Y. Lu, X. X. Zhao, Z. Zhu, M. S. Song, N. L. Gao, Y. S. Wang, Z. F. Ma, W. D. Shi, Y. S. Yan and H. J. Dong, *Catal. Sci. Technol.*, 2016, **6**, 6513–6524.

26 C. Lai, M. M. Wang, G. M. Zeng, Y. G. Liu, D. L. Huang, C. Zhang, R. Z. Wang, P. Xu, M. Cheng, C. Huang, H. P. Wu and L. Qin, *Appl. Surf. Sci.*, 2016, **390**, 368–376.

27 Y. Y. Wu, Y. M. Dong, X. F. Xia, X. Liu and H. X. Li, *Appl. Surf. Sci.*, 2016, **364**, 829–836.

28 L. X. Chen, X. Y. Wang, W. H. Lu, X. Q. Wu and J. H. Li, *Chem. Soc. Rev.*, 2016, **45**, 2137–2211.

29 R. N. Liang, J. W. Ding, S. S. Gao and W. Qin, *Angew. Chem., Int. Ed.*, 2017, **56**, 6833–6837.

30 Z. Y. Lu, F. Chen, M. He, M. S. Song, Z. F. Ma, W. D. Shi, Y. S. Yan, J. Z. Lan, F. Li and P. Xiao, *Chem. Eng. J.*, 2014, **249**, 15–26.

31 X. T. Shen, L. H. Zhu, G. X. Liu, H. W. Yu and H. Q. Tang, *Environ. Sci. Technol.*, 2008, **42**, 1687–1692.

32 R. Yang, Y. X. Liu, X. Y. Yan, S. M. Liu and H. S. Zheng, *J. Mater. Chem. A*, 2016, **4**, 9807–9815.

33 S. J. Li, S. S. Cao, M. J. Whitcombe and S. A. Piletsky, *Prog. Polym. Sci.*, 2014, **39**, 145–163.

34 Z. Zhu, Y. Yu, H. Huang, X. Yao, H. J. Dong, Z. Liu, Y. S. Yan, C. X. Li and P. W. Huo, *Catal. Sci. Technol.*, 2017, **7**, 4092–4104.

35 H. Zhu, X. L. Wang, X. X. Liu and X. R. Yang, *Adv. Mater.*, 2012, **24**, 6524–6529.

36 C. Q. Yuan, X. H. Liu, M. Y. Jia, Z. X. Luo and J. N. Yao, *J. Mater. Chem. A*, 2015, **3**, 3409–3415.

37 M. R. Huang, Q. Y. Peng and X. G. Li, *Chem.–Eur. J.*, 2006, **12**, 4341–4350.

38 A. J. Cheah, W. S. Chiu, P. S. Khiew, H. Nakajima, T. Saisopa, P. Songsiriritthigul, S. Radiman and M. A. A. Hamid, *Catal. Sci. Technol.*, 2015, **5**, 4133–4143.

39 A. Meng, J. Xing, Z. J. Li, Q. Wei and Q. D. Li, *J. Mol. Catal. A: Chem.*, 2016, **411**, 290–298.

40 J. Jiang, H. Li and L. Z. Zhang, *Chem.–Eur. J.*, 2012, **18**, 6360–6369.

41 W. Zhang, L. Zhou and H. P. Deng, *J. Mol. Catal. A: Chem.*, 2016, **423**, 270–276.

42 K. Yuan, L. Chen and Y. W. Chen, *Chem.–Eur. J.*, 2015, **21**, 11899–11906.

43 C. Boitard, A. Rollet, C. Ménager and N. Griffete, *Chem. Commun.*, 2017, **53**, 8846–8849.

44 Y. S. Wang, Z. Y. Lu, Z. Zhu, X. X. Zhao, N. L. Gao, D. D. Wang, Z. F. Hua, Y. S. Yan, P. W. Huo and M. S. Song, *RSC Adv.*, 2016, **6**, 51877–51887.

45 R. Z. Wang, D. L. Huang, Y. G. Liu, Z. W. Peng, G. M. Zeng, C. Lai, P. Xu, C. Huang, C. Zhang and X. M. Gong, *RSC Adv.*, 2016, **6**, 106201–106210.

46 X. L. Li, H. J. Lu, Y. Zhang and F. He, *Chem. Eng. J.*, 2017, **316**, 893–902.

47 J. H. Tong, L. L. Bo, Z. Li, Z. Q. Lei and C. G. Xia, *J. Mol. Catal. A: Chem.*, 2009, **307**, 58–63.

48 Z. Y. Lu, M. He, L. L. Yang, Z. F. Ma, L. Yang, D. D. Wang, Y. S. Yan, W. D. Shi, Y. Liu and Z. F. Hua, *RSC Adv.*, 2015, **5**, 47820–47829.

49 K. F. Ortega, S. Anke, S. Salamon, F. Özcan, J. Heese, C. Andronescu, J. Landers, H. Wende, W. Schuhmann, M. Muhler, T. Lunkenbein and M. Behrens, *Chem.–Eur. J.*, 2017, **23**, 12443–12449.

50 K. K. Senapati, C. Borgohain and P. Phukan, *Catal. Sci. Technol.*, 2012, **2**, 2361–2366.

51 X. X. Pan, L. Q. Yan, C. G. Li, R. J. Qu and Z. Y. Wang, *Chem. Eng. J.*, 2017, **326**, 1197–1209.

52 H. H. Ji, L. Lyu, L. L. Zhang, X. Q. An and C. Hu, *Appl. Catal., B*, 2016, **199**, 230–240.

53 Q. Wu, G. E. Chen, W. G. Sun, Z. L. Xu, Y. F. Kong, X. P. Zheng and S. J. Xu, *Chem. Eng. J.*, 2017, **313**, 450–460.

54 L. Q. Jing, Y. G. Xu, S. Q. Huang, M. Xie, M. Q. He, H. Xu, H. M. Li and Q. Zhang, *Appl. Catal., B*, 2016, **199**, 11–22.

55 X. G. Li, M. R. Huang and W. Duan, *Chem. Rev.*, 2002, **102**, 2925–3030.

56 P. F. Zhang, L. Wang, S. Z. Yang, J. A. Schott, X. F. Liu, S. M. Mahurin, C. L. Huang, Y. Zhang, P. F. Fulvio, M. F. Chisholm and S. Dai, *Nat. Commun.*, 2017, **8**, 15020.

57 Y. W. Jiang, J. L. Carvalho-de-Souza, R. C. S. Wong, Z. Q. Luo, D. Isheim, X. B. Zuo, A. W. Nicholls, I. W. Jung, J. P. Yue, D. J. Liu, Y. C. Wang, V. D. Andrade, X. H. Xiao, L. Navrazhnykh, D. E. Weiss, X. Y. Wu, D. N. Seidman, F. Bezanilla and B. Z. Tian, *Nat. Mater.*, 2016, **15**, 1023–1030.

58 G. T. Pan, C. M. Huang, P. Y. Peng and T. C. K. Yang, *Catal. Today*, 2011, **164**, 377–383.

59 W. S. Chang, Y. C. M. Li, T. W. Chung, Y. S. Lin and C. M. Huang, *Appl. Catal., A*, 2011, **407**, 224–230.